
OBJECT MANIPULATION OF THE VARIABLE TOPOLOGY TRUSS SYSTEM

Andrew Jang-Ho Bae

Department of Mechanical Engineering
University of Nevada, Las Vegas
Las Vegas, NV 89154
andrew.bae@unlv.edu

Myeongjin Choi

Advanced Robotics Research Center
Research Institute of AI Robotics
Korea Institute of Machinery and Materials
Daejeon 34103
aud0109@kimm.re.kr

Haorui Li

RealMan Robotics Co., Ltd.
Beijing, 100043
lihaorui0331@gmail.com

Mark Yim

Department of Mechanical Engineering
and Applied Mechanics
University of Pennsylvania
Philadelphia, PA 19104
yim@seas.upenn.edu

TaeWon Seo

Department of Mechanical Engineering
Hanyang University
Seoul, 04763
taewonsoe@hanyang.ac.kr

May 14, 2026

ABSTRACT

This paper presents an object manipulation strategy for the Variable Topology Truss (VTT) system, a truss robot that comprises actuated truss members connected by passive spherical joints. Although truss robots were originally proposed as rapidly deployable manipulators, manipulation strategy has not been studied thoroughly. To enable manipulation, we introduce a hybrid control framework that regulates position and force concurrently without explicit decoupling. At the actuator level, each member employs a sensor-based force feedback controller to generate the desired axial forces despite high actuator friction. At the task level, the forces applied at the end-effector nodes are produced by computing the required member forces using a static model of the VTT. We evaluate force-tracking performance through experiments on both a single member module and the full VTT system. Finally, we demonstrate object manipulation using two representative configurations and quantitatively assess combined position and force tracking performance. Experimental results confirm that the proposed approach enables consistent and reliable object manipulation with the VTT system.

Keywords Modular robot · Truss robot · Manipulation, · Hybrid position-force control

1 Introduction

Truss robot systems have been studied for a considerable to exploit their versatility and flexibility. These systems comprise prismatic joints as truss member modules and are connected together by passive spherical joints. The first truss robot system applications were as a space-deployable manipulator system [1] including a hardware prototype [2]. Later studies focused on the use of truss robot systems for mobile exploration [3, 4, 5].

Although truss robot systems have been proposed for use as deployable manipulators, their manipulation capabilities have not yet been well demonstrated. Several early studies on truss robot systems presented kinematic analysis and trajectory planning algorithms for manipulation [6, 7]. Based on these studies, Chirikjian and Burdick performed a 2-dimensional truss robot maneuver and showed obstacle avoidance and manipulation [8]. Recent studies also focused on trajectory planning for truss robot systems [9, 10]. Usevitch et al. proposed a truss-like robotic system made of soft materials and proposed a manipulation method that involves grabbing objects between the soft edges of the structure

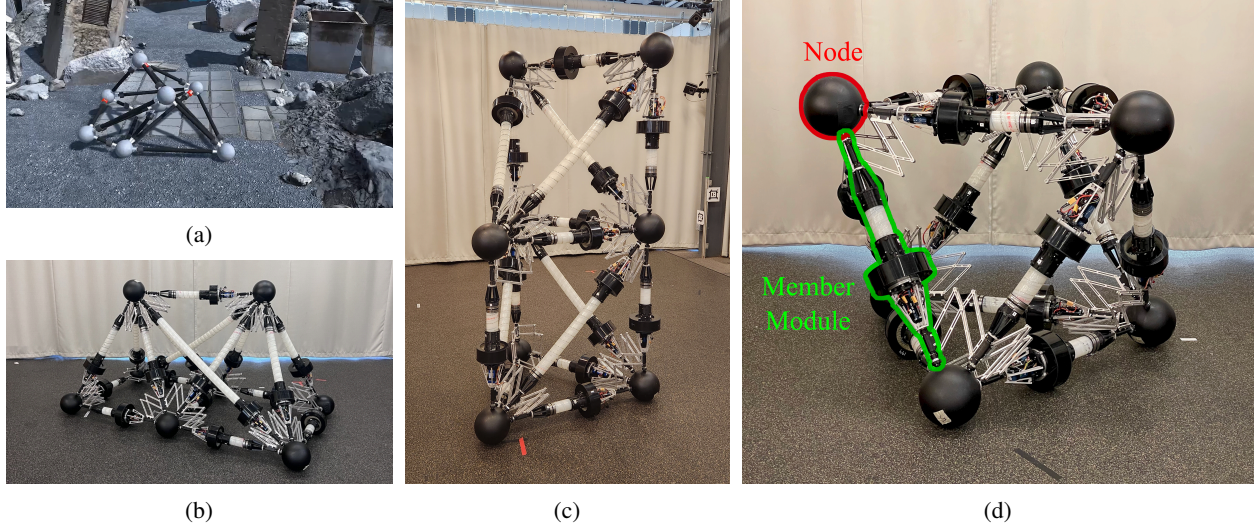


Figure 1: The conceptual rendering and hardware prototype of the VTT system; (a) 3D-rendered scene of search-and-rescue operation of the VTT system; (b) Tent configuration of the VTT system; (c) Tower configuration of the VTT system; (d) Octahedron configuration of the VTT system.

[11, 12]. Although the proposed untethered soft robot is not a typical rigid truss robot system, the study demonstrated the potential for manipulation of truss-like robots.

Force and position control, especially in task space, is crucial for performing object manipulation. In truss-robot systems, task-space control refers to regulating the position and/or force of a target node. Although task space force control is clearly beneficial for object manipulation with truss robot systems, no studies have specifically focused on its implementation. Several previous studies focused on the dynamic modeling and analyzed manipulator-level force of truss robot systems with simulation results [13, 14, 15]. Cubero and Billingsley investigated force control for a truss robot system, but their experiments were limited to a single pneumatic actuator [16].

The Variable Topology Truss (VTT) system is a truss robotic system that includes the capability to self-reconfigure its topology [17]. The original goal was to deploy in unstructured environments, such as damaged buildings and provide structural support for search and rescue operations in case of collapse, Figure 1a. By using spiral zippers as actuators for the truss member modules, the VTT system can achieve significant size changes that were not possible in previous truss robot systems [18, 19]. To enable effective search-and-rescue operations, locomotion planning is part of the task sequence [20, 21, 22, 23]. Other important tasks that can take advantage of the VTT system’s ability to reconfigure its topology [24]. Object manipulation tasks in the search and rescue context include delivering medical supplies or removing debris. One challenge for VTT for object manipulation comes from the spiral zipper’s high friction and the VTT system’s complex kinematics and statics which leads to difficulty developing a controller that can track VTT contact point position and force [19].

This paper presents an object manipulation strategy for the VTT system based on a hierarchical hybrid position/force control. First, we develop force controllers at both the actuator level and the task-space level. Because the spiral zipper actuator has high friction, each actuator uses sensor-based force feedback to generate the desired axial force. Based on the static model of the VTT system, we formulate a method to compute the member forces required to produce a desired task-space force at the target nodes. The force tracking performance of a single actuator and the VTT system are tested with multiple experiments. Two representative configurations are examined: a tetrahedral topology, representing the simplest fully-constrained structure, and a pyramid topology, which is the simplest over-constrained system. Force control experimental results show that the force tracking performance is reliable for both fully and over-constrained truss structures.

Object manipulation requires simultaneous regulation of position and force. Therefore, we propose a hybrid control strategy that achieves concurrent position and force control without explicit decoupling. This approach enables the VTT system to simultaneously track position and force along the same direction, which is not possible with decoupled control. We proposed and experimentally validated a manipulation method that using two VTT nodes to grasp and transport an object. The manipulation performance of the VTT system is validated with two different configurations, double tetrahedron and octahedron with internal nodes. Experimental results show that the hybrid controller achieves

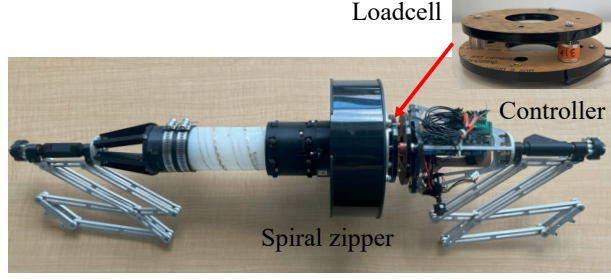


Figure 2: Picture of a member module in the VTT system

consistent and reliable manipulation for both cases. Given the VTT’s intended role in real-world disaster response, the proposed hierarchical hybrid control framework forms a foundation for autonomous and adaptive manipulation in unstructured environments.

2 Materials and Methods

2.1 Variable Topology Truss System

The VTT system is a truss robot system that can drastically change its size and reconfigure its topology. As shown in Figure 1, the VTT system can achieve various configurations by assembling the truss modules in different ways. A *member module* is a truss element of the VTT system. A *node* is a passive spherical joint that connects member modules. In Figure 1d, a member module is highlighted in green, while a node is highlighted in red.

2.1.1 Member Module

Each member module is equipped with a linear actuator, sensors, a controller, and a battery. Therefore, each module can operate independently and be easily assembled in different configuration without interfering with other modules. A loadcell assembly is attached for force sensing of each truss element of the VTT system. Figure 2 presents a photograph of an individual member module.

Each member module includes a spiral zipper actuator for linear actuation. The spiral zipper actuator is a linear actuator capable of achieving an exceptionally large extension ratio [18]. The spiral zipper operates by winding up a long flat band (0.05” thick nylon), which helps minimize the actuator’s retracted length. For the VTT system, the spiral zipper design has been modified to ensure compatibility with the VTT system, as shown in Figure 3. A nylon band column is rotated by a motor (118 RPM HD Premium Planetary Gear Motor, ServoCity) in the center of the column, while the length of the actuator is measured with two photointerrupters (OPB628). The two photointerrupters are positioned with a 90° phase offset to detect the direction of band motion.

2.1.2 Control System Summary

The control architecture of the VTT system is summarized in Figure 4. Each member module uses an ESP32 microcontroller (ESP32-PICO-KIT v4) that executes the low-level control loop. Using loadcell feedback, the low-level controller regulates the actuator to produce the commanded axial force. The controller also estimates the member length using two photointerrupters by counting the teeth on the spiral zipper band passing the sensor. The ESP32s on the member modules communicate wirelessly using the ESP-NOW protocol with a master ESP32 connected to a host computer. The ESP-NOW protocol provides lightweight, low-latency communication compared to standard Wi-Fi.

The high-level controller is implemented in ROS2 and runs on the host computer. It receives state information from each module via the master ESP32 and computes the desired force commands for the member modules based on the measured module states and the required position and force at the target node. These force commands are then transmitted back to the member modules through the master ESP32. The details of the high-level and low-level controllers are presented in the following sections.

2.1.3 VTT Kinematic Analysis

The length between two connected nodes (l_i) can be expressed as follows from Figure 5:

$$l_i = |(\mathbf{p}_i - \mathbf{p}_j)|, \quad (1)$$

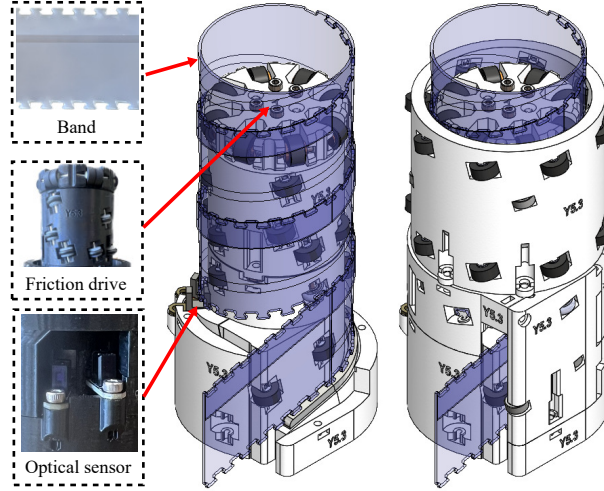


Figure 3: The CAD modeling of the spiral zipper actuator

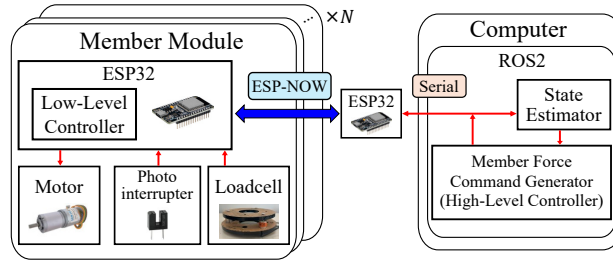


Figure 4: The control architecture of the VTT system

where $\mathbf{p}_i = [p_{ix}, p_{iy}, p_{iz}]^\top$ denotes the position vector of i -th node.

We define the stacked node position vector $\mathbf{P} = [\mathbf{p}_1^\top, \dots, \mathbf{p}_N^\top]^\top$ and the member length vector $\mathbf{L} = [l_1, \dots, l_M]^\top$, where N and M denote the numbers of nodes and members. By combining the relation between node positions and member lengths in VTT can be expressed as follows.:

$$\mathbf{L} = f(\mathbf{P}), \quad (2)$$

where $f(x)$ is a function derived from Eq. 1. By differentiating Eq. 2 with respect to node position, the inverse kinematics equation can be found from Figure 5:

$$\dot{\mathbf{L}} = \mathbf{J}\dot{\mathbf{P}}, \quad (3)$$

where matrix \mathbf{J} is the inverse Jacobian of the VTT, mapping node velocities to member length velocities.

2.1.4 VTT Static Analysis

Based on previous studies, the motion of the VTT system can be considered quasi-static. The relation between the internal forces and the nodal forces can be derived using the transpose of the inverse Jacobian matrix.

$$\mathbf{F} = \mathbf{J}^\top \boldsymbol{\lambda} + \mathbf{W}, \quad (4)$$

where $\mathbf{F} = [\mathbf{F}_1^\top, \dots, \mathbf{F}_N^\top]^\top$ is the stacked vector of nodal forces, while $\boldsymbol{\lambda} = [\lambda_1, \dots, \lambda_M]^\top$ denotes the vector of internal forces. \mathbf{J} is the inverse Jacobian matrix derived in Eq. 3. $\mathbf{W} = [\mathbf{w}_1^\top, \dots, \mathbf{w}_N^\top]^\top$ is the vector of the external forces applied to each node includes gravitational forces.

Let E_k denote the set of member indices connected to node k . While the index $i \in E_k$ denotes the indices of the members that are connected to the node k , the required member force vector $\boldsymbol{\lambda}$ to generate the desired force \mathbf{F}_{des} at

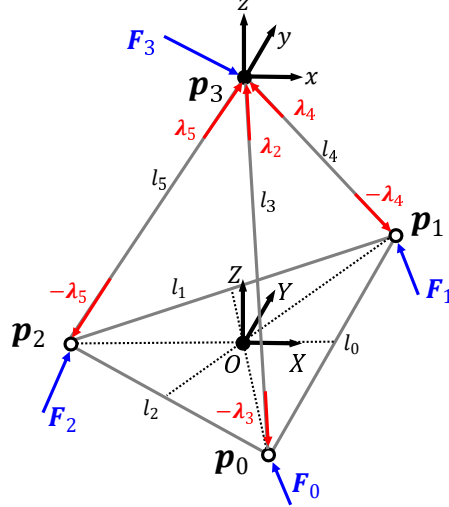


Figure 5: Mathematical schematics of the VTT system in a tetrahedral configuration. Black circles represent the nodes of the VTT, and gray lines represent the Spiral-Zipper beams.

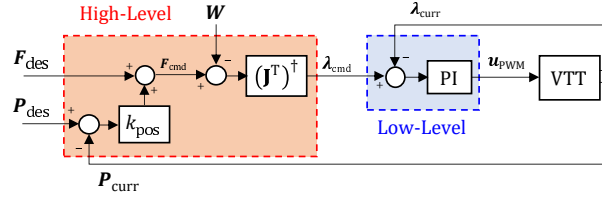


Figure 6: Block diagram of the hybrid position/force control for object manipulation using the VTT system.

node k can be calculated as follows:

$$\lambda_k = \left(\mathbf{J}_k^\top \right)^\dagger \left(\mathbf{F}_{des} - \mathbf{W}_k \right) \quad (5)$$

where λ_k is the vector of member forces λ_i , which is the forces of the members connected to the node k . \mathbf{J}_k is the submatrix of the inverse Jacobian \mathbf{J} formed by selecting the columns corresponding to $i \in E_k$. \mathbf{W}_k denotes the external force vector applied to node k . The symbol \dagger denotes the Moore-Penrose pseudoinverse.

2.2 Hierarchical Hybrid Control of the VTT System

To perform grasping and manipulation with the VTT system, the nodal position and contact force must be controlled simultaneously. We propose a hierarchical hybrid controller that achieves concurrent position and force control without explicit decoupling, enabling tracking of position and force along the same direction. Figure 6 presents the overall control structure. The high-level controller computes the desired nodal force command to track both position and force and maps this command to the corresponding member force commands using the system statics. The low-level controller then drives each actuator to generate the required member forces received from the high-level controller.

2.2.1 High-Level Controller

The high-level controller generates a force command for the target node to simultaneously track the desired force and position. The commanded nodal force is computed by summing the desired force and a proportional feedback term based on the position error, as follows:

$$\mathbf{F}_{cmd} = \mathbf{F}_{des} + k_{pos} \left(\mathbf{P}_{des} - \mathbf{P}_{curr} \right), \quad (6)$$

where \mathbf{F}_{des} is the stacked vector of desired nodal forces applied to the environment. \mathbf{P}_{des} denotes the stacked desired node positions, and \mathbf{P}_{curr} is the stacked current node positions. k_{pos} is the proportional gain for position control part which can be interpreted as the stiffness gain that converts end-effector node position deviations into equivalent stiffness forces. The member forces command λ_{cmd} required to generate the nodal force \mathbf{F}_{cmd} can be derived from Eq. 5 by substituting the command force vector \mathbf{F}_{cmd} into \mathbf{F}_{des} , and the weight of nodes and members compensation vector \mathbf{W}

into W_k . λ_{cmd} is the stacked vector of a member force command $\lambda_{\text{cmd},i}$ for each member. This way, the control law generates an equivalent force to tracking position and force simultaneously, enabling high level unified force-based command synthesis.

2.2.2 Low-Level Controller

The low-level control directly interfaces with VTT's actuation system to execute the high-level force commands. A Proportional-Integral (PI) controller is implemented to regulate the actuator output. The controller can be expressed as follows:

$$u_{\text{PWM}} = k_P e_\lambda + k_I \int e_\lambda dt, \quad (7)$$

where u_{PWM} is the pulse width modulation (PWM) input for controlling the motor. $e_\lambda = \lambda_{\text{cmd}} - \lambda_{\text{curr}}$ is the error between the desired member force λ_{cmd} , derived from the high-level controller, and the current member force λ_{curr} , measured from the loadcell assembly.

2.2.3 Remark on Decoupling and Stability

Most position-force hybrid controllers decouple the force and position directions into orthogonal subspaces using selection operators [25, 26]. In contrast, by avoiding this decoupling, the system can control force and position along the same direction simultaneously, but with the cost of increased tracking error. Assuming quasi-static motion, each channel reduces to a proportional or impedance-type feedback loop. Therefore, all control components have exponentially stable error dynamics in its respective subspace for positive gains. By adjusting the stiffness gain k_f , we can adjust control strength between position and force to keep the closed-loop tracking errors bounded. Since this study focuses on demonstrating experimental feasibility, we select k_f to prioritize position tracking accuracy over force tracking performance.

2.3 Object Manipulation of the VTT System

In addition to controlling the position of end effectors in contact with an object we would like to control internal forces on the object to ensure a positive grasp. We propose a hierarchical hybrid control for object manipulation with the VTT system. This way the VTT system can control the object that results in both position as well as static controlled forces. To verify the objective manipulation performance, we propose two configurations of VTT.

The double-tetrahedron configuration is the most intuitive and simplest setup for object manipulation. It consists of two identical tetrahedral VTTs. The system manipulates an object by pushing it with the two top nodes, as shown in Figures 7a and 7b. Although the double-tetrahedron configuration is easy to control, it has several limitations, such as a restricted workspace and difficulty representing realistic manipulation scenarios. Therefore, the double-tetrahedron configuration is used for detailed data generation. Multiple trajectories were executed with this configuration, and the resulting position and force data were analyzed.

The octahedron configuration uses two internal tetrahedrons to manipulate a target object, as shown in Figures 7c and 7d. The two internal nodes press the object from opposite sides to hold it in place. Because this configuration better represents realistic manipulation scenarios, we used it to test practical object manipulation tasks.

3 Results

The control performance of the hybrid controller is evaluated experimentally before testing manipulation. First, a force-tracking experiment on a single spiral zipper actuator is conducted to verify actuator-level force control performance. Next, we perform force-tracking experiments with two different VTT configurations to assess whether the node-level force control performance is sufficient for manipulation.

After validating the force-tracking performance, we evaluate manipulation performance using both the double-tetrahedron and octahedron configurations. In the double-tetrahedron configuration, we primarily test combined position and force tracking over multiple trajectories. In the octahedron configuration, the manipulation task is designed as a more practical, application-oriented scenario.

3.1 Force Control of a Single Spiral Zipper

To measure the force applied by a spiral zipper actuator, we constructed a dedicated test fixture, as shown in Figure 8a. The test fixture consists of a fixed vertical mounting structure and a load cell at the free end to measure compressive

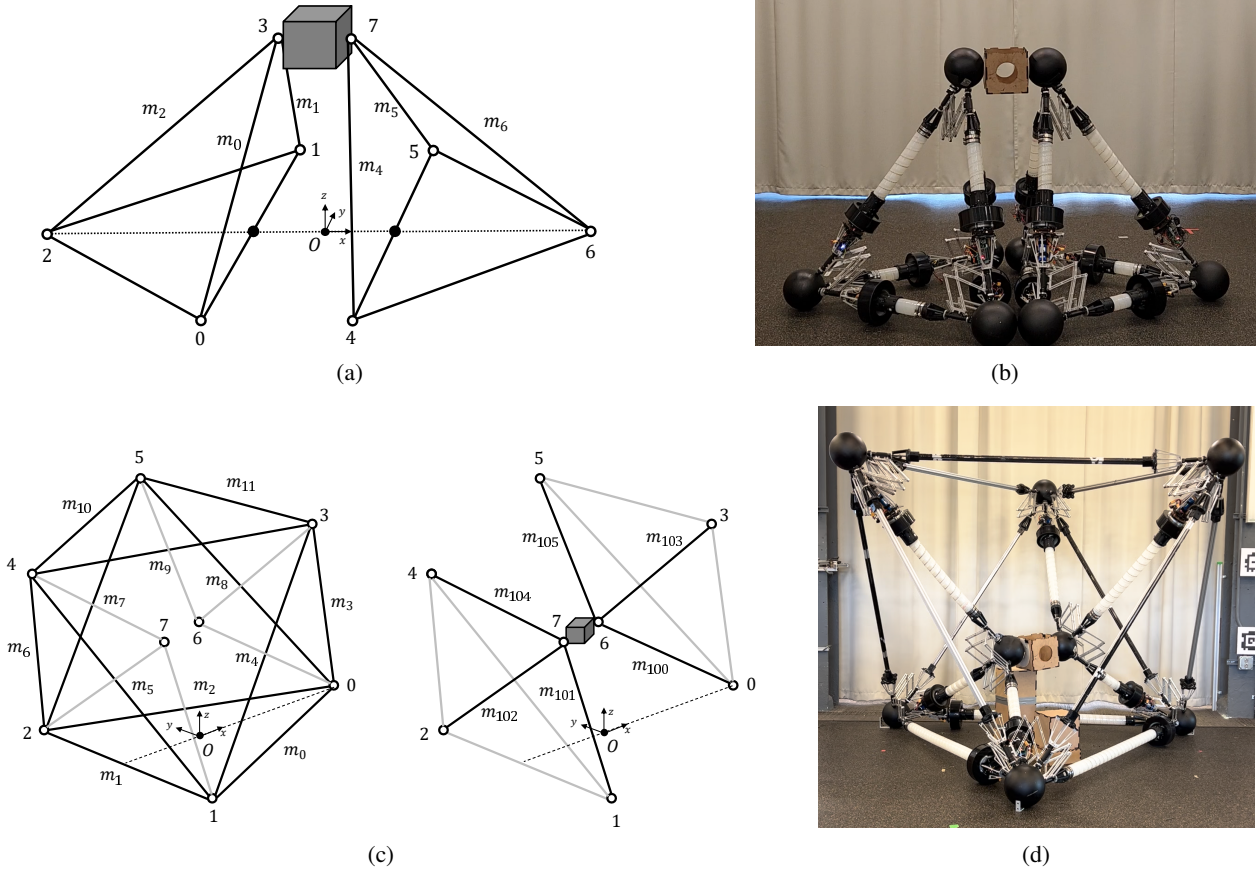


Figure 7: Two manipulation configuration of VTT. (a) Schematic of the double tetrahedral configuration; (b) Picture of the double tetrahedral configuration; (c) Schematic of the octahedral configuration; (d) Picture of the octahedral configuration.

forces. We used a force signal that increases at 10 N/s until it reaches the desired maximum to avoid unnecessary oscillations. The maximum values of the ramp inputs were set between 10 N and 200 N .

The force response results are summarized in Figure 9. During the force-ramping phase, the output force exhibits a steeper slope at lower target forces, despite the constant input rate (Figure 9a). Minor errors appear only in specific low-force regions, caused by the dead zone of the spiral zipper actuator. The dead zone is caused by design characteristics of the spiral zipper’s internal friction-drive mechanism, which requires a relatively high actuation torque to initiate motion. This dead zone prevents motion under low input signals, resulting in step-like behavior in the low-force range. During the force-holding phase, the module consistently sustains the desired force with less than 5% error across all tested ranges. These results confirm that the spiral zipper actuator can reliably generate and maintain axial forces, demonstrating its suitability for integration into the VTT system.

3.2 Force Control of the VTT System

We could not find any previous studies that conducted an experimental validation of force-control performance for VGT or similar truss robot systems. Most prior studies on manipulation have relied solely on simulation to evaluate motion and force performance. Several studies have experimentally demonstrated force control only at the single-actuator level [15]. For evaluating the force-tracking performance of the full VTT system, external load cells were mounted near the target node to measure the applied forces, as shown in Figure 8b and 8c. We selected tetrahedron and pyramid configurations as reference cases. The tetrahedron configuration is the simplest rigid, fully constrained truss structure, while the pyramid configuration allows us to assess force control performance in an over-constrained truss system. We used similar force signals used for a single spiral zipper testing, the force signal increases at 10 N/s until it reaches the desired maximum value. The maximum values of the force inputs were set between 10 N and 50 N . We tested force generation in both the horizontal (x) and vertical (z) directions.

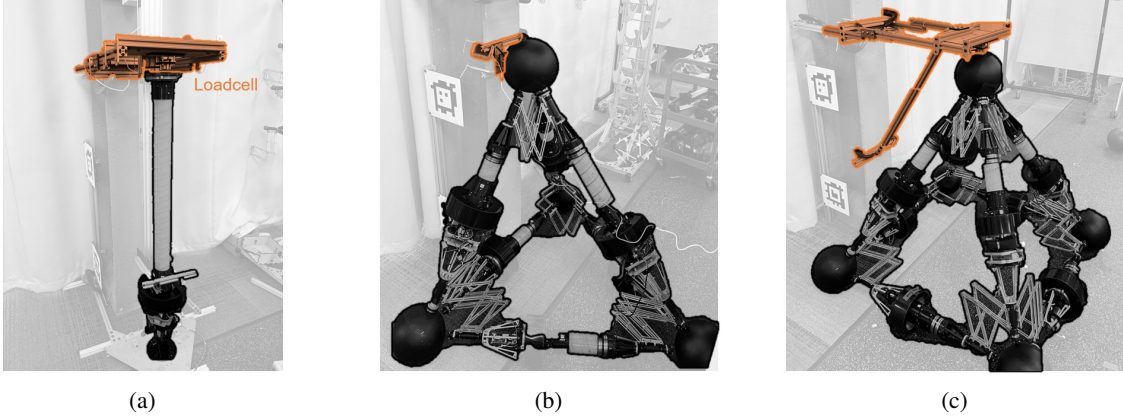


Figure 8: Experimental setups for force control evaluation. Orange components indicate the force measurement devices equipped with load cell. (a) Testbench for Spiral Zipper; (b) Testbench for tetrahedron topology VTT; (c) Testbench for pyramid topology VTT.

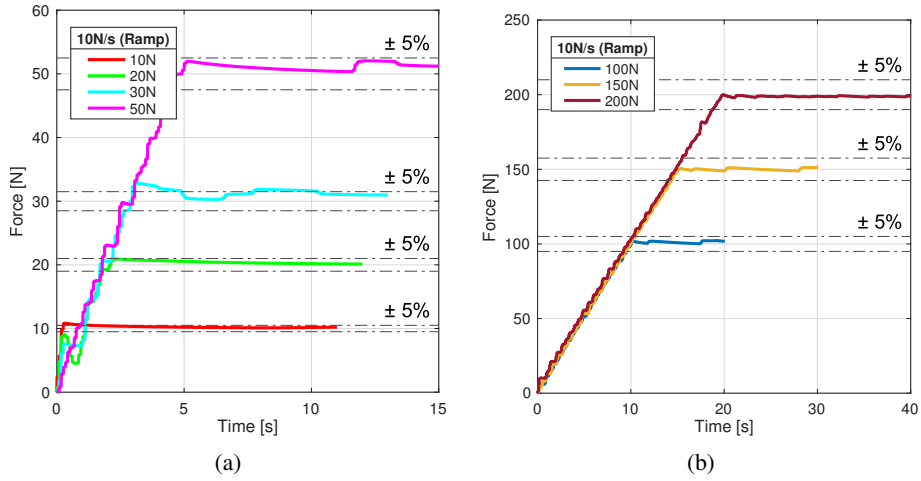


Figure 9: Experimental results of force control of the Spiral-Zipper under ramp input signals of 10 N/s. (a) Force responses in the range of 10–50 N. (b) Force responses in the range of 100–200 N.

3.2.1 Tetrahedral Configuration

The results of the force-tracking experiments in the tetrahedral configuration are shown in Figure 10. In both the horizontal and vertical directions, the applied force remains within 5% of the target value during the force-holding phase.

For the x -direction, a significant overshoot is observed at lower target forces as shown in Figure 10a. We attribute this behavior to the combined effects of the actuator dead zone and friction in the node joints. Here, the spiral zipper actuators begin to move abruptly only after the input current exceeds a certain threshold, which leads to overshoot.

In the z -direction, the overall performance was more stable, with smaller errors and less overshoot, as shown in Figure 10b. The observed step-like behavior is also caused by the dead zone of the spiral zipper actuator, particularly under increasing compressive loads. Despite these behaviors, the VTT system in the tetrahedral configuration demonstrated reliable force-tracking performance in both directions, showing the effectiveness of the proposed control method in a fully constrained system.

3.2.2 Pyramid Configuration

The experimental results of force tracking in the pyramid topology are shown in Figure 10. This configuration is selected to evaluate force control performance in an over-constrained structure. In both directions, the error during

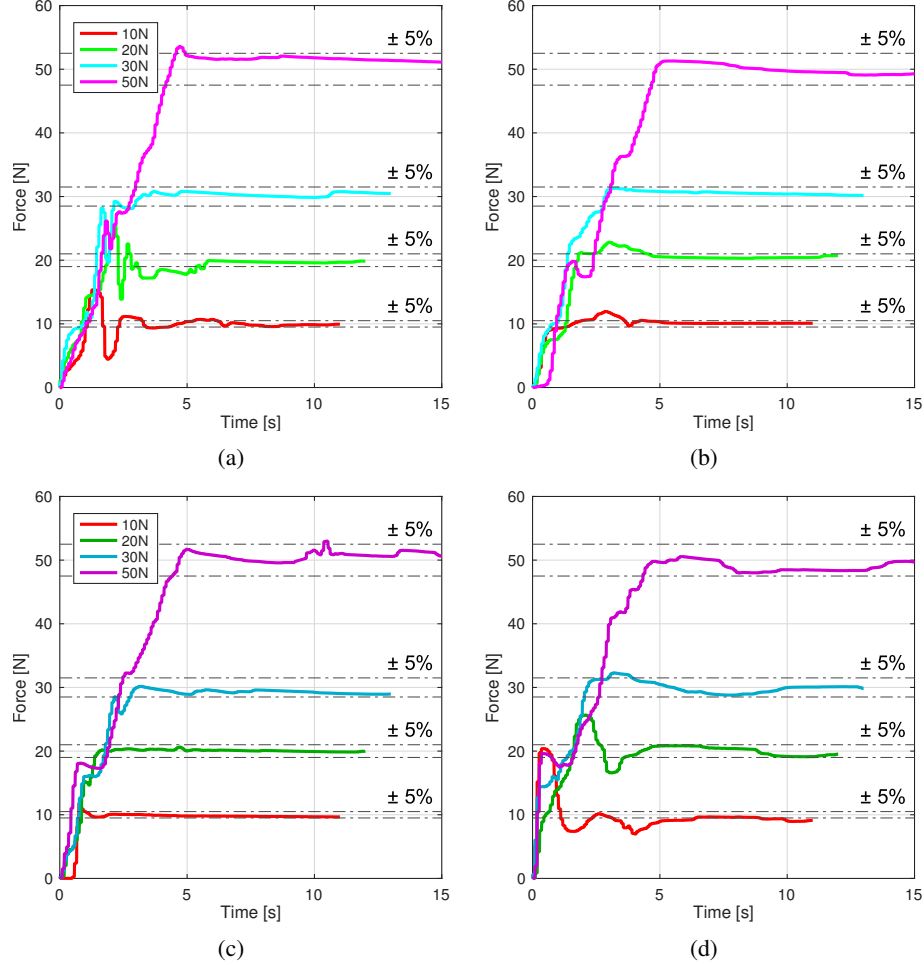


Figure 10: Experimental results of force control in the tetrahedral topology under target forces ranging from 10–50 N. (a)–(b) Force responses for tetrahedron topology along the x - and z -axes. (c)–(d) Force responses for pyramid topology along the x - and z -axes.

the force-holding phase remains within approximately 5% across all target force levels, indicating overall stable performance.

Similar to the tetrahedron configuration results, a significant overshoot is observed, particularly in the z direction. The overshoot-related errors are larger in the pyramid configuration, which we attribute to the combined effects of the spiral zipper actuator dead zone and internal forces caused by the over-constrained structure. We considered the overshoot observed in the pyramid configuration to be acceptable given the over-constrained nature of the structure. Therefore, we conclude that the proposed hybrid position/force control method is successful.

3.3 Object Manipulation

3.3.1 Double Tetrahedral Configuration

We could not find any prior studies have investigated two-node grasping with a VGT system. Using the double-tetrahedron configuration, we evaluated the position and force tracking performance over the following trajectories:

- Linear motion
 1. x -axis motion between +0.5 m and -0.5 m
 2. y -axis motion between +0.35 m and -0.35 m
 3. y -axis motion from 0 to +0.5 m and back to the initial position
- Circular motion

1. Circular trajectory in xy plane (radius 0.2 m)
2. Circular trajectory in yz plane (radius 0.2 m)
3. Circular trajectory in xz plane (radius 0.2 m)
4. Circular trajectory in xyz space (radius 0.2 m)

The target object is a wooden cube with dimensions $20\text{ cm} \times 20\text{ cm} \times 20\text{ cm}$ and a mass of 931 g. Silicone pads attached to the sides of the object increase the friction coefficient between the node spheres and the object. The grasping force is set to 60 N for all cases, which means that each grasping node applies 30 N of force to the target object. By using the hierarchical hybrid controller, the VTT system is controlled to follow the trajectory while maintaining the grasping force applied from node 3 and node 7 in Figure 7a.

The position and force tracking performance data for all experiments are summarized in Table 1 and Table 2. Each experiment is repeated three times, and the root mean square error (RMSE) values are obtained by averaging the results of the three trials. In all seven experiments, the position RMSE remains within centimeters, which is reasonably accurate for manipulation. The force RMSE is larger compared to the commanded grasping force. This is due to the gain settings of the hierarchical hybrid controller, because the controller does not decouple the position and force control inputs, there is a trade-off between position and force tracking performance with higher importance set to position accuracy.

Figure 11 and xyz plane in Figure 12 show detailed plots. 11, both the position and force data remain within a small error range for the xy circular trajectory experiment. The xyz circular trajectory results indicate a phase delay in the z position tracking. In the case of z -position control, all three members must apply compressive or tensile forces toward each other. This generates internal forces due to friction in the spherical joints at the nodes, reducing the effective force available for adjusting the z position, which results in decreasing the maximum achievable z displacement. In addition, the spiral zipper actuator dead zone, adds positioning error. The combination of these two issues results in a phase delay in the z -direction motion.

Figure 13 shows the snapshots of the circular movement experiment on xyz plane.

Table 1: Experimental results for line trajectories along different axes.

Axis	x (m) ^a	y (m) ^b	z (m) ^c	F (N) ^d
x-axis	0.0321	0.0049	0.0197	7.30
y-axis	0.0143	0.0421	0.0295	13.87
z-axis	0.0118	0.0051	0.1372	5.67

^a RMSE in x -direction.

^b RMSE in y -direction.

^c RMSE in z -direction.

^d RMSE of desired internal force.

Table 2: Experimental results for the circular trajectory executed on different planes.

Plane	x (m) ^a	y (m) ^b	z (m) ^c	F (N) ^d
xy	0.0244	0.0236	0.0095	5.05
yz	0.0100	0.0181	0.0824	10.35
xz	0.0188	0.0093	0.0648	9.18
oblique	0.0109	0.0173	0.0689	9.15

^a RMSE in x -direction.

^b RMSE in y -direction.

^c RMSE in z -direction.

^d RMSE of desired internal force.

3.3.2 Octahedral Configuration

With the octahedron configuration, we evaluate a configuration that could be used for both locomotion and manipulation making the task-space more interesting [23]. Here, the VTT moves one box from one pile to another pile located 0.5 m away, then places a second box on top of the first. Both box piles are located inside the octahedral VTT structure when the manipulation begins.

The target objects are cube-shaped boxes, each weighing 309 g. The grasping force is set to 12 N, and the average manipulation speed is 0.01 m/s. The manipulation sequence is as follows:

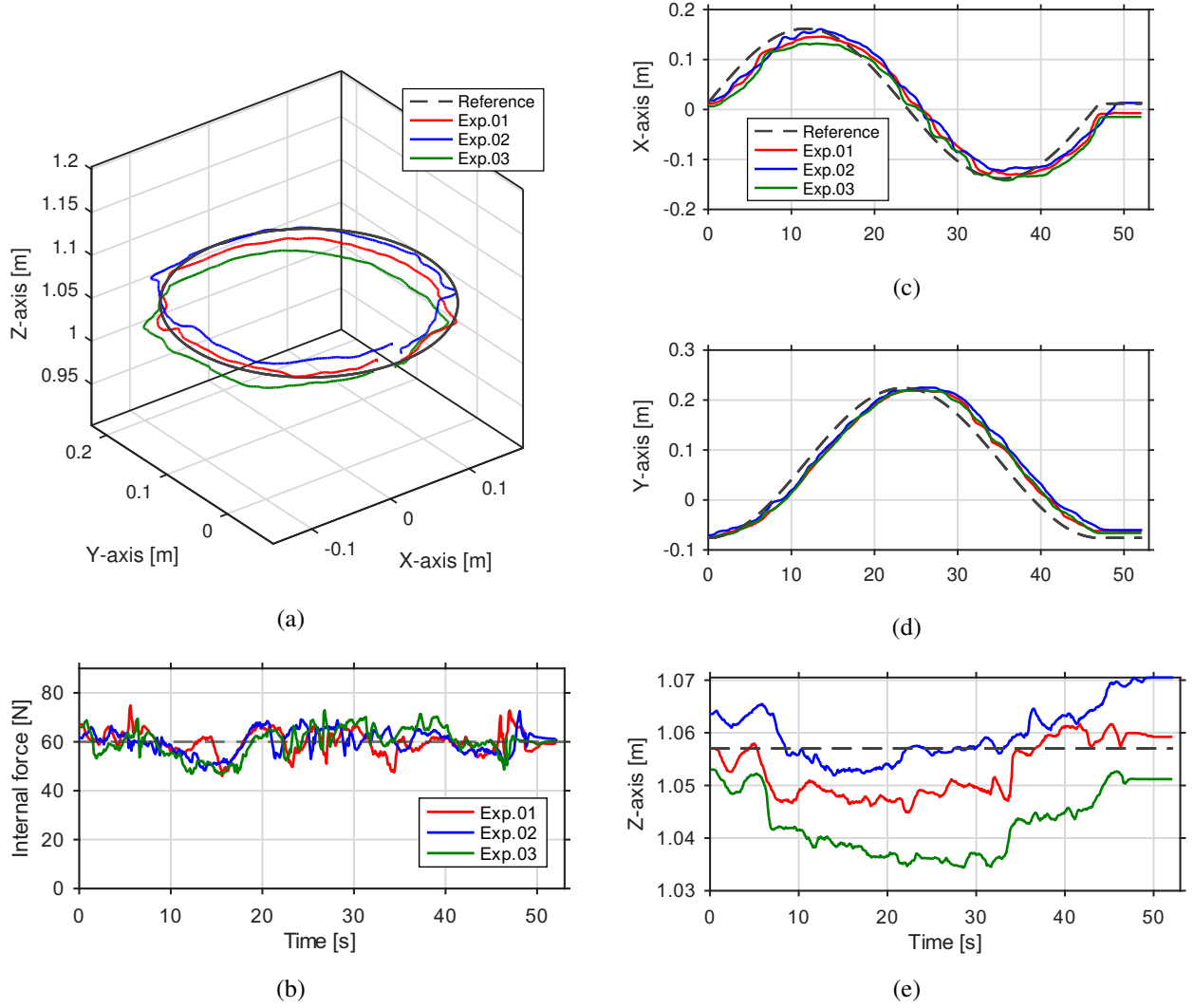


Figure 11: Experimental results of xy plane grab manipulation with two tetrahedron VTT. (a) 3D trajectory. (b) Internal force. (c) X-axis tracking result. (d) Y-axis tracking result. (e) Z-axis tracking result.

- Move to the initial position using pure length control
- Grasp the first box with 12 N grasping force
- Move in the z direction by 0.08 m for 10 s
- Move in the y direction by 0.5 m for 52 s
- Move in the z direction by -0.4 m for 42.5 s
- Release the first box
- Return to the second grasping position using pure position control
- Grasp the second box with 12 N grasping force
- Move in the z direction by 0.1 m for 8.5 s
- Move in the y direction by 0.5 m for 52.5 s
- Release the second box

Figure 14 shows snapshots of the two-box transfer experiment, and a supplementary video is provided. The manipulation takes about 4 min 50 s to complete. This octahedron-based manipulation experiment demonstrates that VTT

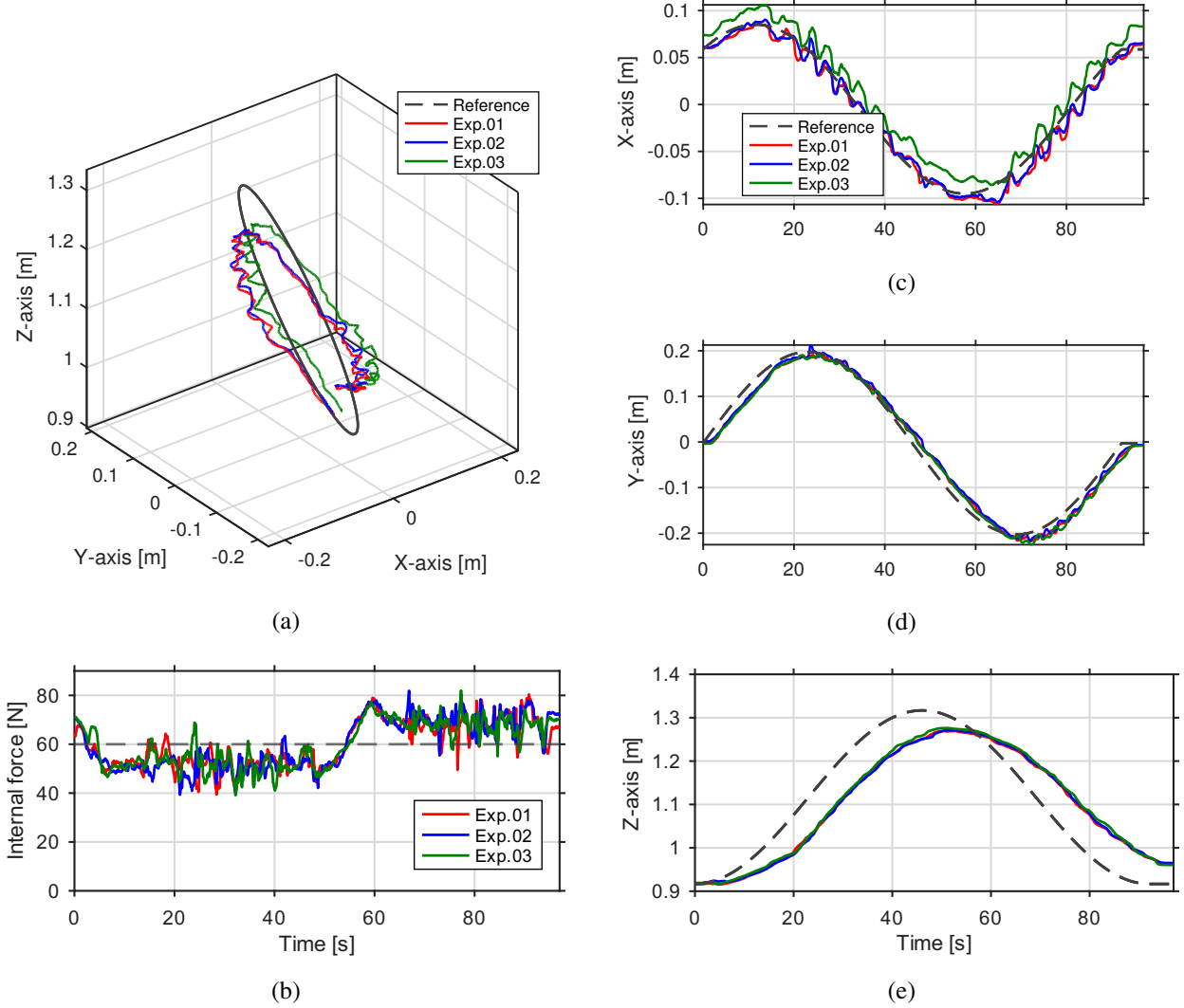


Figure 12: Experimental results of xyz plane grab manipulation with two tetrahedron VTT. (a) 3D trajectory. (b) Internal force. (c) X-axis tracking result. (d) Y-axis tracking result. (e) Z-axis tracking result.

manipulation is repeatable, as the system successfully moves two objects consecutively. With this demonstration, it is easy to see that the VTT can manipulate and carry objects through locomotion [23].

4 Conclusion

In this paper, we proposed the concept of performing manipulation with the VTT system and demonstrated its feasibility. To enable manipulation, we developed a hierarchical hybrid controller capable of regulating position and force simultaneously without decoupling. On the hardware side, we improved the spiral zipper actuator design to achieve the required strength and tolerance. Because the spiral zipper actuator exhibits high friction and a large gear ratio, we implemented sensor-based force control for each truss member module. The force-tracking performance of the spiral zipper actuators was validated in multiple configurations. Manipulation performance was evaluated using the double-tetrahedron configuration, where we showed that the position tracking accuracy is sufficient for reliable manipulation while maintaining the grasping force. Finally, we demonstrated a practical manipulation scenario with the octahedron configuration.

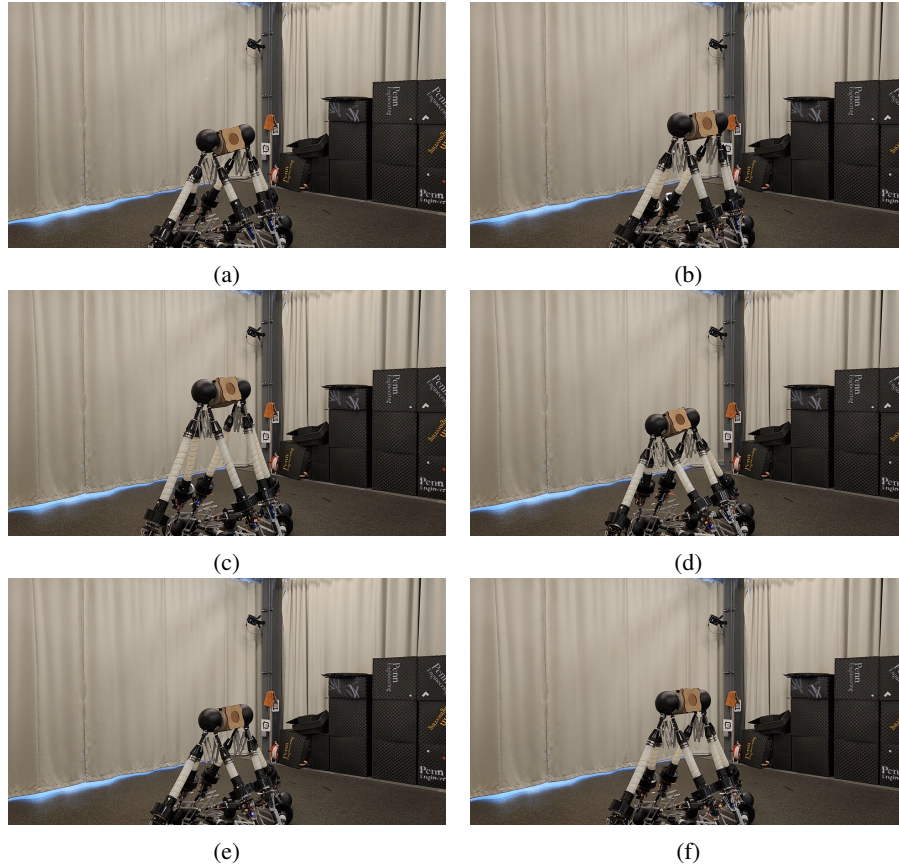


Figure 13: Snapshots of the double tetrahedron VTT manipulation experiment. (a) 0:00 min; (b) 0:18 min; (c) 0:42 min; (d) 1:16 min; (e) 1:40 min; (f) 1:57 min.

5 Funding Statement

This research was supported by the MOTIE (Ministry of Trade, Industry, and Energy) in Korea, under the Human Resource Development Program for Industrial Innovation(Global) (P0017306, Global Human Resource Development for Innovative Design in Robot and Engineering) supervised by the Korea Institute for Advancement of Technology (KIAT).

6 Acknowledgment

Thanks to Henry Zhao for assisting the VTT programming and experiments.

References

- [1] Koryo Miura, Hiroshi Furuya, and Kenichi Suzuki. Variable geometry truss and its application to deployable truss and space crane arm. *Acta Astronautica*, 12(7-8):599–607, 1985.
- [2] Peter C Hughes, Wayne G Sincarsin, and Kieran A Carroll. Trussarm—a variable-geometry-truss manipulator. *Journal of Intelligent Material Systems and Structures*, 2(2):148–160, 1991.
- [3] Gregory J Hamlin and Arthur C Sanderson. Tetrobot: A modular approach to parallel robotics. *IEEE Robotics & Automation Magazine*, 4(1):42–50, 1997.
- [4] Woo Ho Lee and Arthur C Sanderson. Dynamic rolling locomotion and control of modular robots. *IEEE Transactions on robotics and automation*, 18(1):32–41, 2002.

- [5] Steven Curtis, Matthew Brandt, Greg Bowers, Gary Brown, Cynthia Cheung, Caner Cooperider, Mike Desch, Noah Desch, John Dorband, Kyle Gregory, et al. Tetrahedral robotics for space exploration. In *2007 IEEE Aerospace Conference*, pages 1–9. IEEE, 2007.
- [6] Frank Naccarato and Peter Hughes. Inverse kinematics of variable-geometry truss manipulators. *Journal of Robotic Systems*, 8(2):249–266, 1991.
- [7] Gun-Shing Chen and Ben K Wada. Adaptive truss manipulator space crane concept. *Journal of Spacecraft and Rockets*, 30(1):111–115, 1993.
- [8] Gregory S Chirikjian and Joel W Burdick. A hyper-redundant manipulator. *IEEE Robotics & Automation Magazine*, 1(4):22–29, 1994.
- [9] Yanchun Zhao, Shiqiang Hu, and Yongsheng Yang. Inverse kinematics for the variable geometry truss manipulator via a lagrangian dual method. *International Journal of Advanced Robotic Systems*, 13(6):1729881416666779, 2016.
- [10] Dingdong Shen and Shiqiang Hu. Space variable geometry truss manipulator experimental system design and implementation. In *Proceedings of the 2017 International Conference on Mechatronics Systems and Control Engineering*, pages 15–19, 2017.
- [11] Nathan S Usevitch, Zachary M Hammond, Mac Schwager, Allison M Okamura, Elliot W Hawkes, and Sean Follmer. An untethered isoperimetric soft robot. *Science Robotics*, 5(40), 2020.
- [12] Zachary M Hammond, Nathan S Usevitch, and Sean Follmer. Grasp analysis and manipulation kinematics for isoperimetric truss robots. In *2021 IEEE International Conference on Robotics and Automation (ICRA)*, pages 6140–6146. IEEE, 2021.
- [13] Hiroshi Furuya and Kenichi Higashiyama. Dynamics of closed linked variable geometry truss manipulators. *Acta astronautica*, 36(5):251–259, 1995.
- [14] BA Boutin, Arun K Misra, and VJ Modi. Dynamics and control of variable-geometry truss structures. *Acta Astronautica*, 45(12):717–728, 1999.
- [15] Sven Rost, Yevgen Sklyarenko, Frank Schreiber, and Walter Schumacher. Design of a modular hydraulically driven variable geometry truss structure and its nonlinear controller architecture for highly dexterous motion. In *8th International Fluid Power Conference*, 2012.
- [16] Samuel N Cubero and John Billingsley. Force, compliance and position control for a space frame manipulator. In *Proceedings Fourth Annual Conference on Mechatronics and Machine Vision in Practice*, pages 124–129. IEEE, 1997.
- [17] Alexander Spinos, Devin Carroll, Terry Kientz, and Mark Yim. Topological reconfiguration planning for a variable topology truss. *Journal of Mechanisms and Robotics*, 13(4):040901, 2021.
- [18] Foster Collins and Mark Yim. Design of a spherical robot arm with the spiral zipper prismatic joint. In *2016 IEEE international conference on robotics and automation (ICRA)*, pages 2137–2143. IEEE, 2016.
- [19] Seohyeon Lee, Sahoan Ahn, Devin Carroll, Mark Yim, and TaeWon Seo. Slip modeling and simulation of spiral zipper friction-driven prismatic actuator. In *2021 IEEE/RSJ International Conference on Intelligent Robots and Systems (IROS)*, pages 9347–9352. IEEE, 2021.
- [20] Sumin Park, Eugene Park, Mark Yim, Jongwon Kim, and TaeWon Seo. Optimization-based nonimpact rolling locomotion of a variable geometry truss. *IEEE Robotics and Automation Letters*, 4(2):747–752, 2019.
- [21] Sumin Park, Jangho Bae, Seohyeon Lee, Mark Yim, Jongwon Kim, and TaeWon Seo. Polygon-based random tree search planning for variable geometry truss robot. *IEEE Robotics and Automation Letters*, 5(2):813–819, 2020.
- [22] Jangho Bae, Sumin Park, Mark Yim, and Taewon Seo. Polygon-based random tree search algorithm for a size-changing robot. *IEEE Robotics and Automation Letters*, 2021.
- [23] Jangho Bae, Inha Park, Mark Yim, and TaeWon Seo. Locomotion planning of a truss robot on irregular terrain. In *2023 IEEE/RSJ International Conference on Intelligent Robots and Systems (IROS)*, pages 824–829. IEEE, 2023.
- [24] Alexander Spinos and Mark Yim. Towards a variable topology truss for shoring. In *2017 14th International Conference on Ubiquitous Robots and Ambient Intelligence (URAI)*, pages 244–249. IEEE, 2017.
- [25] Chae H An and John M Hollerbach. The role of dynamic models in cartesian force control of manipulators. *The International Journal of Robotics Research*, 8(4):51–72, 1989.
- [26] William D Fisher and M Shahid Mujtaba. Hybrid position/force control: A correct formulation. *The International journal of robotics research*, 11(4):299–311, 1992.

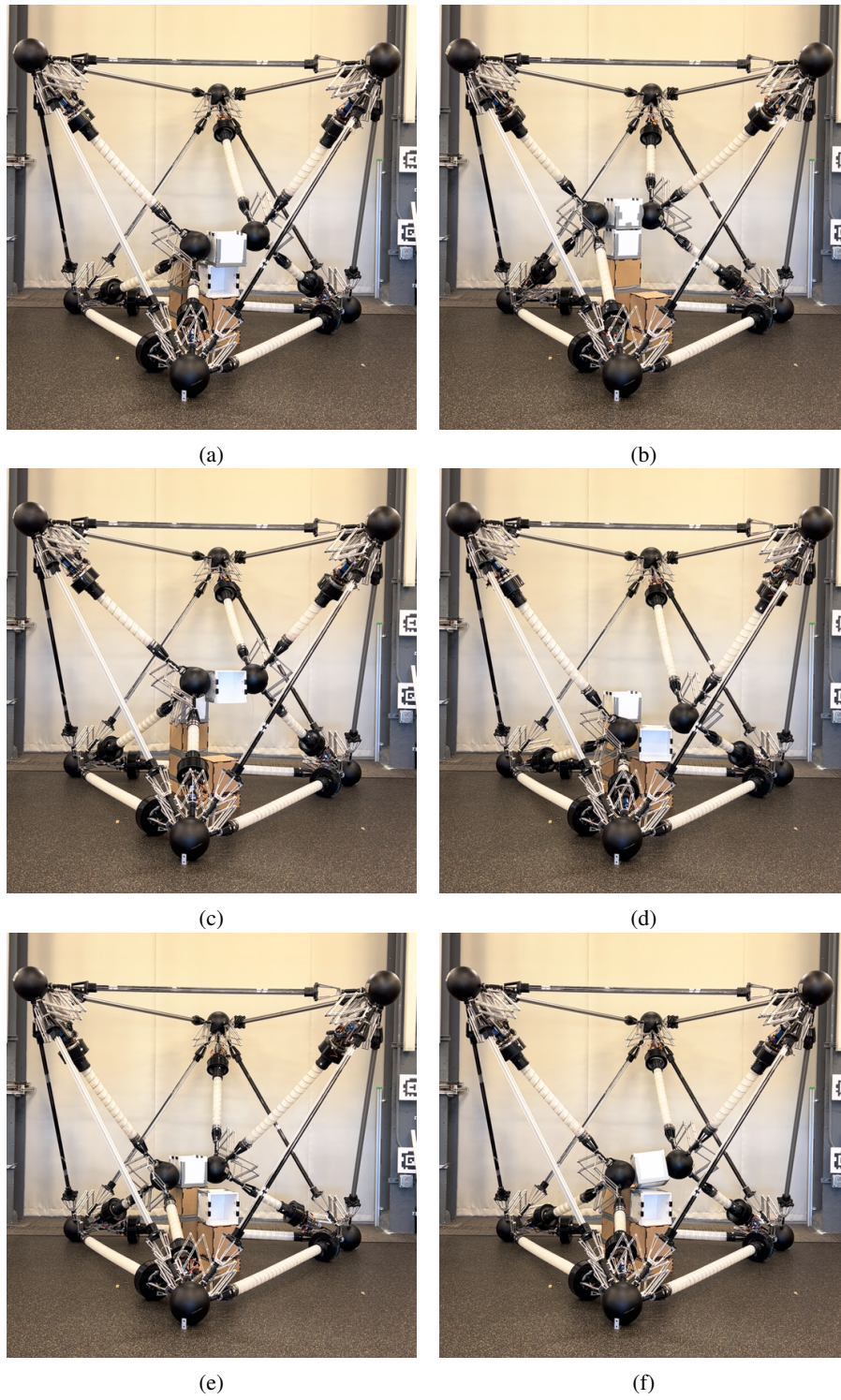


Figure 14: Snapshots of the double tetrahedron VTT manipulation experiment. (a) 0:00 min; (b) 1:13 min; (c) 1:52 min; (d) 3:31 min; (e) 4:23 min; (f) 4:40 min.